

Structural monitoring of the onset of excited-state aromaticity in a liquid crystal phase

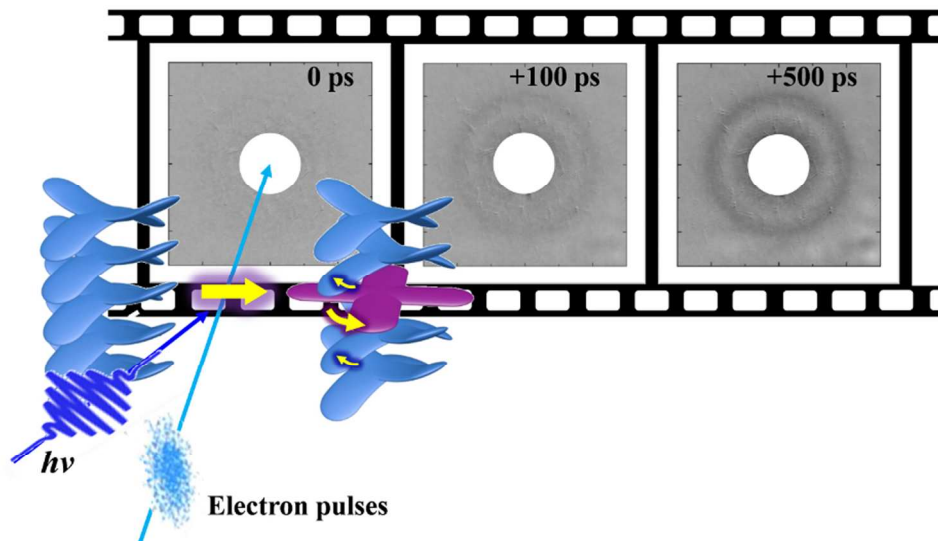
Masaki Hada, Shohei Saito, Sei'ichi Tanaka, Ryuma Sato, Masahiko Yoshimura, Kazuhiro Mouri, Kyohei Matsuo, Shigehiro Yamaguchi, Mitsuo Hara, Yasuhiko Hayashi, Fynn Roehricht, Rainer Herges, Yasuteru Shigeta, Ken Onda, and R. J. Dwayne Miller

J. Am. Chem. Soc., **Just Accepted Manuscript** • DOI: 10.1021/jacs.7b08021 • Publication Date (Web): 16 Oct 2017

Downloaded from <http://pubs.acs.org> on October 16, 2017

Just Accepted

"Just Accepted" manuscripts have been peer-reviewed and accepted for publication. They are posted online prior to technical editing, formatting for publication and author proofing. The American Chemical Society provides "Just Accepted" as a free service to the research community to expedite the dissemination of scientific material as soon as possible after acceptance. "Just Accepted" manuscripts appear in full in PDF format accompanied by an HTML abstract. "Just Accepted" manuscripts have been fully peer reviewed, but should not be considered the official version of record. They are accessible to all readers and citable by the Digital Object Identifier (DOI®). "Just Accepted" is an optional service offered to authors. Therefore, the "Just Accepted" Web site may not include all articles that will be published in the journal. After a manuscript is technically edited and formatted, it will be removed from the "Just Accepted" Web site and published as an ASAP article. Note that technical editing may introduce minor changes to the manuscript text and/or graphics which could affect content, and all legal disclaimers and ethical guidelines that apply to the journal pertain. ACS cannot be held responsible for errors or consequences arising from the use of information contained in these "Just Accepted" manuscripts.



TOC graphic

82x44mm (300 x 300 DPI)

Structural monitoring of the onset of excited-state aromaticity in a liquid crystal phase

Masaki Hada^{1*†}, Shohei Saito^{2,3*†}, Sei'ichi Tanaka⁴, Ryuma Sato⁵,
Masahiko Yoshimura⁶, Kazuhiro Mouri⁶, Kyohei Matsuo⁶, Shigehiro Yamaguchi⁶,
Mitsuo Hara⁷, Yasuhiko Hayashi¹, Fynn Röhricht⁸, Rainer Herges⁸, Yasuteru Shigeta^{5*},
Ken Onda^{9*}, R. J. Dwayne Miller^{10,11}

¹Graduate School of Natural Science and Technology, Okayama University, Okayama 700-8530, Japan.

²Graduate School of Science, Kyoto University, Kyoto 606-8502, Japan.

³JST-PRESTO, Kawaguchi 332-0012, Japan.

⁴School of Science, Tokyo Institute of Technology, Yokohama 226-8502, Japan.

⁵Center for Computational Sciences, University of Tsukuba, Tsukuba 305-8577, Japan.

⁶Graduate School of Science, Nagoya University, Nagoya 464-8602, Japan.

⁷Graduate School of Engineering, Nagoya University, Nagoya 464-8603, Japan.

⁸Otto Diels-Institute for Organic Chemistry, Christian-Albrechts University Kiel, Kiel 24119, Germany.

⁹Department of Chemistry, Faculty of Science, Kyushu University, Fukuoka 819-0395, Japan.

¹⁰Max Planck Institute for the Structure and Dynamics of Matter, Center for Free Electron Laser Science, Hamburg Centre for Ultrafast Imaging, University of Hamburg, Hamburg 22761, Germany.

¹¹Departments of Chemistry and Physics, University of Toronto, Toronto M5S 3H6, Canada.

†These authors contributed equally to this work.

ABSTRACT: Aromaticity of photoexcited molecules is an important concept in organic chemistry. Its theory, Baird's rule for triplet aromaticity since 1972, gives the rationale of photoinduced conformational changes and photochemical reactivities of cyclic π -conjugated systems. However, it is still challenging to monitor the dynamic structural change induced by the excited-state aromaticity, particularly in condensed materials. Here we report direct structural observation of a molecular motion and a subsequent packing deformation accompanied by the excited-state aromaticity. Photoactive liquid crystal (LC) molecules featuring a π -expanded cyclooctatetraene core unit are orientationally ordered but loosely packed in a columnar LC phase, and therefore a photoinduced conformational planarization by the excited-state aromaticity has been successfully observed by time-resolved electron diffractometry and vibrational spectroscopy. The structural change took place in the vicinity of excited molecules, producing a twisted stacking structure. A nanoscale torque driven by the excited-state aromaticity can be used as the working mechanism of new photoresponsive materials.

Introduction

The concept of excited-state aromaticity was first introduced from a theoretical viewpoint. In 1972, Baird predicted the photoinduced aromaticity of cyclic $4n\pi$ -electron systems in their lowest triplet state (T_1)¹. Baird aromaticity is in sharp contrast to the commonly observed Hückel aromaticity of cyclic $(4n+2)\pi$ -electron systems in their singlet ground state (S_0)². On the basis of Baird's rule, photoinduced conformational changes and photoreactivities of cyclic π -conjugated systems are rationally explained in a variety of organic compounds³. Compared to the other anomalous " $4n\pi$ aromaticities", Möbius aromaticity⁴ and three-dimensional stacked-ring aromaticity⁵, experimental clues of Baird aromaticity have been found from earlier stage⁶ mainly because the excited-state aromaticity is reflected in the results of photoreactions of common π -conjugated systems. Until recently, most of the experimental insight for the excited-state aromaticity has been indirectly obtained on the basis of their photoreactivities.^{3b} As latest advances, structural

changes during aromaticity reversal (Hückel \leftrightarrow Baird) in T_1 and S_1 have been analyzed by time-resolved absorption and IR spectroscopies using expanded porphyrins and their metal complexes,⁷ and the energetics of Baird aromaticity has been quantified by circular dichroism spectroscopy with photoirradiation of a chiral COT derivative.⁸ However, direct structural observation of Baird aromatic species has been still limited to spectroscopy. This situation is different from the study of Möbius and stacked-ring aromaticities, whose structural analyses have been provided by single-crystal X-ray diffractometry^{4c-e,g,5c}. The main difficulty derives from the requirement for the real-time diffraction analysis of short-lived species in the excited state. In this work, we overcome this difficulty by the combination of the synthesis of a $4n\pi$ liquid crystal (LC) molecule and the ultrafast electron-diffraction analysis. We report a direct structural evidence of a conformational planarization of π -expanded cyclooctatetraene (COT) and a subsequent packing deformation in a columnar LC phase, accompanied by the excited-state aromaticity of its $4n\pi$ electron circuit.

This work also includes an advancement in the method of structural characterization of photoresponsive liquid crystals. In spite of remarkable progress in the time-resolved diffractometry using ultrabright and ultrashort-pulsed X-ray⁹ and electron¹⁰ sources, the application has been limited to the structural characterization of simple isolated molecules or single crystals in excited state. In this study, we have characterized the structural dynamics of photoexcited LC thin films by the combinational use of time-resolved electron diffractometry and molecular dynamics (MD) simulations. Since the electron scattering from organic samples is stronger than the X-ray scattering, diffraction change can be monitored in real time with sufficient intensity even for such a thin film that UV excitation light can penetrate the whole materials.

Results and Discussion

Molecular design.

Molecular motion of the 8π COT ring has attracted attention not only from the viewpoint of aromaticity but from the viewpoint of materials science. COT has been utilized for a broad range of applications such as a triplet quencher of fluorescent conjugated polymers¹¹, an additive for improving the photostability of organic fluorophores in imaging techniques¹², a molecular viscosity probe¹³ and a light-melt adhesive¹⁴. The conformational planarization of the photoexcited COT ring is a key motion in their working mechanism. Here we synthesized a columnar LC molecule (see Figures S1–2) that is composed of the π -expanded COT (π -COT) core unit with typical dendritic alkyl chain moieties¹⁵ (Figure 1a). The saddle-shaped π -COT skeleton was selected as a photoactive core unit of the LC molecule, because it has the following unique features: 1) high conformational flexibility due to the small internal steric hindrance between the neighboring thiazole rings with the head-to-tail connection¹⁶, 2) stacking ability to form a well-defined columnar structure despite its nonplanar molecular frame¹⁶, and 3) 8π electron system at the central COT ring that is expected to undergo a photoinduced conformational change into a flat form owing to the excited-state aromaticity.¹⁷ In this photoactive columnar LC system, the orientationally ordered saddle-shaped molecules afford structural information for the time-resolved diffraction analysis, and the loosely packed structure allows the intramolecular conformational planarization and the following intermolecular packing deformation in the vicinity of photoexcited molecules.

Characterization of columnar liquid crystal.

The π -COT-based material exhibited a columnar LC phase between 15 and 84°C (Figure S3), which enabled the time-resolved structural analysis of the LC phase to be performed at room temperature. Using polarized optical microscopy (POM) observations, the LC texture of the material was confirmed using crossed Nicols (bright regions in the inset of Figure 1b). Figure 1b shows the XRD pattern of the LC phase obtained using Cu $K\alpha$ radiation (see Figure S4 and Table S1). The LC structure was characterized as a rectangular columnar form of $C2/m$, in which the saddled molecules align on top of one other

(Figure 1c). The XRD analysis yielded lattice parameters of $a = 61.6 \text{ \AA}$ and $b = 41.7 \text{ \AA}$. The intermolecular distance in the stacked column along the c -axis was obscured by a broad diffraction peak ($2\theta \approx 20^\circ$; $d \approx 4.4 \text{ \AA}$) originating from the dendritic alkyl chain moiety. This situation is quite common for typical columnar LC materials¹⁴.

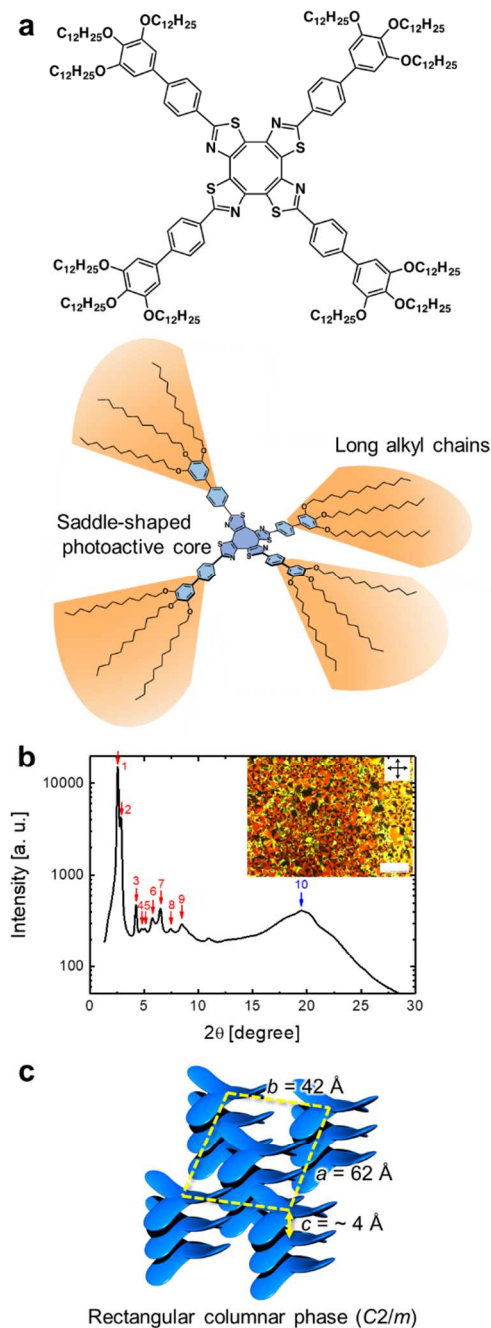


Figure 1: Molecular structure and lattice parameters of the liquid crystal. **a**, Chemical structure and stereoscopic view of the π -COT-based LC molecule with a saddle shaped conformation in the ground state (S_0). **b**, The static X-ray diffraction pattern with several peaks indicated by arrows. Blue arrow particularly indicates the (001) peak. The inset figure shows POM image of the LC thin film at 80°C under crossed Nicols. The white scale bar demonstrates 200 μm . **c**, The lattice parameters in the LC phase. Rectangular columnar phase of $C2/m$ was assigned according to the extinction rule.

Conformational planarization in the excited state.

The photoinduced dynamics of the columnar LC material consists of a sequence of structural motions at different scales: first, a conformational change at the molecular level (Figures 2–4) and, second, a subsequent deformation of the local packing structure around the photoexcited molecules in the π -stacked columns (Figures 5–8). Inspired by the predictions of the triplet aromaticity of parent COT^{3a,b,17}, the saddle-to-flat conformational change in the excited state of the π -COT core unit was calculated using density functional theory (DFT) quantum chemical calculations. Photochemical formation of the triplet state of COT requires a multiple process. Upon excitation of the tub-shaped parent COT with D_{2d} symmetry, the higher excited singlet states are formed ($S_0 \rightarrow S_n$) and immediate radiationless decay into the lowest singlet excited state takes place ($S_n \rightarrow S_1$).¹⁸ Then, a rapid intersystem crossing to the triplet state ($S_1 \rightarrow T_1$) is expected (see Figure S31, in which the intersystem crossing through $S_1 \rightarrow T_2 \rightarrow T_1$ scheme has been supported). Although the conformational planarization of COT in the excited state has been studied in relation to the triplet energy transfer,¹⁹ the conformational dynamics in S_1 has never been observed experimentally as far as we know, probably because its lifetime is extremely short. In this context, we performed (TD-)DFT calculations of the π -COT core unit in the ground and excited states. While the S_0 optimized structure takes a saddle conformation with the S–C–C–N torsion angle φ of 37° (Figures 2a,c), the optimized structures in S_1 and T_1 predict flat conformations with $\varphi = 0^\circ$ (Figures 2b,d for T_1 and Figure S21). The CASSCF calculations also indicate the flat conformation in S_1 and T_1 (Figure S27). On the assumption that the intersystem crossing would take place after the saddle-to-flat conformational change in S_1 , the structural optimizations with fixed φ from 0° to 120° in 8° intervals were performed in S_1 (Figure 3a). The resulting energy diagrams indicated that the S_1 energy is significantly lowered as the molecular shape flattens, suggesting spontaneous conformational planarization in the excited state.

Excited-state aromaticity.

Importantly, the pronounced excited-state aromaticity of the T_1 structure was confirmed by standard aromaticity indices, the anisotropy of the induced current density (ACID)²⁰, the nucleus-independent chemical shift (NICS)²¹, and the harmonic oscillator model of aromaticity (HOMA)²². In these analyses, a model structure of π -COT bearing biphenyl groups was investigated. The ACID plot revealed a strong diatropic (aromatic) ring current on the π -COT core unit (Figure 2e and Figure S28). Distinct contribution of the 8π electron circuit was confirmed along the COT ring, while diatropic ring current in the 24π -electron periphery including the thiazole rings is also remarkable. The central COT ring remains uncharged (unlike COT²⁺ or COT²⁻) according to a natural bond orbital (NBO) charge distribution analysis (Figure S23). In relation to this, it has been recently reported that localization/delocalization of excited-state aromaticity depends on each annelated ring system.²³ NICS(1) and

NICS(1)_{zz} values, magnetic criteria for the aromaticity^{21b-d}, were calculated to be –8.04 and –18.24 ppm at the center of the COT ring in the planar T_1 structure at the GIAO-UB3LYP/6-311+G**//UB3LYP/6-31+G* level of theory (see also Figures S24 and S25). By comparison with Baird aromatic D_{8h} COT in T_1 showing NICS(1) = –10.80 and NICS(1)_{zz} = –32.08 ppm at the same GIAO level (with the reported C–C bond length of 1.4063 Å¹⁷, HOMA = 0.91), significant Baird aromaticity of π -COT in T_1 was indicated. On the other hand, the saddle-shaped S_0 structure of π -COT calculated at the GIAO-B3LYP/6-311+G**//B3LYP/6-31+G* level showed NICS(1) = 2.76 and NICS(1)_{zz} = 18.31 ppm. By comparison with Hückel antiaromatic D_{4h} COT in S_0 as a transition state showing NICS(1) = 36.28 and NICS(1)_{zz} = 109.43 ppm (with the reported C–C bond lengths of 1.3510 and 1.4718 Å¹⁷, HOMA = –0.08), nonaromaticity of π -COT in S_0 has been supported.

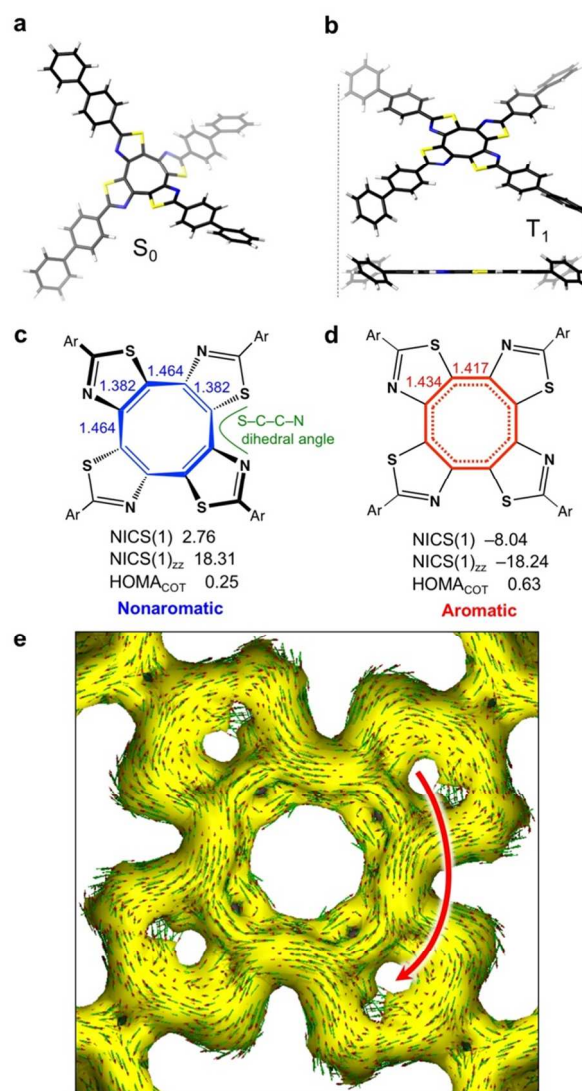


Figure 2: Optimized structures and aromaticity indices of π -COT core unit, in which simplified model (Ar = biphenyl) is treated. **a,b**, DFT optimized structures of S_0 at the B3LYP/6-31G* and of T_1 at the UB3LYP/6-31+G* level of theory. Full optimization was performed with the structural symmetry of C_2 and C_4 , respectively. **c,d**, Bond lengths, NICS(1), NICS(1)_{zz},

and HOMA values on the central COT ring of the optimized structures in S_0 (c) and T_1 (d). NICS calculations were performed with the gauge-independent atomic orbital (GIAO) method at the (U)B3LYP/6-311+G* level of theory. **e**, Enlarged ACID plot for the T_1 optimized structure. Isosurfaces (yellow) and current density vectors (green arrows with red heads) are shown. The current density vectors indicate a diatropic (clockwise) ring current. The complete ACID plot is shown in Figure S28.

The HOMA values, the aromaticity index based on the bond alternation of a focused ring system, are in agreement with the results in the NICS calculations. The C-C bond lengths of the eight-membered COT ring afforded $HOMA_{COT}$ values of 0.65 (aromatic) in T_1 while it was 0.25 (nonaromatic) in S_0 . The aromatic indices in the CASSCF-optimized T_1 and S_0 structures, in which a simplified model structure without the biphenyl groups was treated, also supported the above-mentioned features (Figures S26 and S27). Namely, strong 8π aromaticity of the COT ring in T_1 ($HOMA_{COT} = 0.87$, $NICS(1) = -11.41$ ppm and $NICS(1)_{zz} = -28.83$ ppm) and nonaromaticity in S_0 ($HOMA_{COT} = 0.02$, $NICS(1) = 0.55$ and $NICS(1)_{zz} = 13.85$ ppm) were indicated in the CASSCF optimized structure. In S_1 , significantly small bond alternation is suggested ($HOMA_{COT} = 0.60$), but the degree is not remarkable when compared to T_1 (Figure S26 and S27). These theoretical analyses clearly indicate triplet aromaticity of the π -COT core unit as well as nonaromaticity in S_0 , and it is consistent with the conformational planarization effectively driven by the photoinduced excited-state aromaticity.

Spectroscopies on the molecular dynamics.

We next performed UV-visible absorption spectroscopy and transient transmission spectroscopy at various pump and probe energies on thin films of the π -COT-based LC material in order to confirm the optical excitation and associated photoinduced dynamics. Although the ultrafast dynamics of the parent COT molecule have been studied with ionization/mass spectrometry²⁴, direct structural evidence of the triplet COT species has never been obtained. Figure 3b shows the transient visible transmittance using pump pulse of 4.7 eV ($\lambda = 266$ nm) and probe pulse of approximately 2.1 eV ($\lambda = 500$ –700 nm), respectively (Supplementary Section III). The π -COT molecule that absorbed UV light was immediately excited to a far-from-equilibrium state (S_n) and transferred to the excited state within 2 ps. Thus, the photoexcited π -COT molecule in ~ 100 ps should be relaxed to the lowest excited state; therefore, we will mainly discuss on the photoinduced dynamics of the π -COT molecule on the relevant timescale. The transient transmittance was fitted with the following equation:

$$\Delta T/T = A_1 \exp(-t/\tau_1) + A_2 \exp(-t/\tau_2) + A_3 \quad (1)$$

where the first and second terms indicate exponential decay with the time-constants of τ_1 and τ_2 . The third term suggests the decay of even longer timescale. Once excited in the LC film, most of the molecules returned to S_0 in $\tau_1 = 20$ ps and $\tau_2 = 150$ ps probably through a conical intersection, but a small proportion of the molecules

remained in the excited state for over several-hundred-picoseconds to nanoseconds, which is corresponding to the third term in the equation (1). This long-lifetime species was mainly observed in transient electron diffractometry described in the next Section.

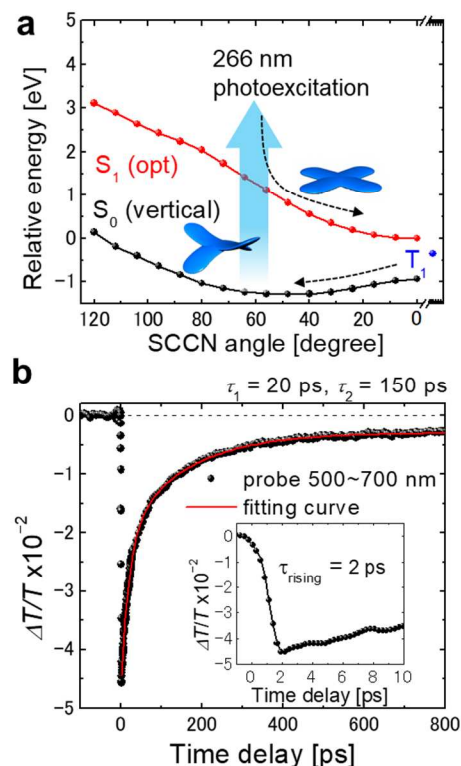


Figure 3: Transient visible transmission spectroscopy of a π -COT-based LC thin film. **a**, Schematic energy diagram in the conformational change of the π -COT core unit bearing biphenyl groups from saddle (S_0) to flat (S_1 and T_1) structures. **b**, Time-resolved visible transmission spectroscopy on the LC thin film using pump and probe light with the energies of 4.7 eV ($\lambda = 266$ nm) and approximately 2.1 eV ($\lambda = 500$ –700 nm), respectively. The rising signal component has a time-constant of 2 ps (as shown in the inset), and the relaxation time-constants are 20 and 150 ps, respectively.

The conformational planarization in the excited state is confirmed by the combination method between time-resolved infrared (IR) vibrational spectroscopy on the LC film and spectral simulation using DFT calculations on the corresponding isolated molecules.^{7e,25} We first compared the ground state FT-IR spectrum to the calculated spectra of the saddle conformer of π -COT model structures in S_0 with different length of alkoxy chains, and confirmed that the propoxyl group ($-OC_3H_7$) is long enough to reproduce the observed spectra (Figure S10 and Table S2). Time-resolved spectra display the evolution of the molecular vibrational modes of the planar π -COT conformer. Figure 4a shows the differential vibrational spectrum at a delay time of 100 ps. After the photoexcitation, several peaks and bleaches in amplitude were observed in the vibrational spectra. The characteristic peaks *e.g.*, at the wavenumbers 1183, 1338 and 1489 cm^{-1} , were well reproduced in the calculated T_1 - S_0 differential vibrational spectrum (Figure 4b), which was obtained by the

1 subtraction of the spectrum at the saddle conformation in
 2 S_0 from the spectrum at the flat conformation in T_1 (see
 3 Figures S12 for more detail). The calculated T_1 - S_0
 4 spectrum showed better agreement with the experiment
 5 than the calculated S_1 - S_0 spectrum, and therefore we
 6 assigned the excited species as T_1 , although the optimized
 7 structures in S_1 and T_1 both take flat conformation and
 8 the possibility of the S_1 observation was not ruled out (Figures
 9 S21 and S27). Figure 4c shows the calculated IR spectrum
 10 of the T_1 structure and colored bars indicate which part
 11 mainly vibrates in the calculated normal mode vibrations
 12 (Figure S13). On the basis of these vibrational assignments,
 13 the peaks at 1183 and 1489 cm^{-1} as indicated by red
 14 dashed lines in Figure 4a are related to the breathing
 15 motions of COT and thiazole rings which are non-active in
 16 saddle shape and active in flat structure. The peaks or
 17 shoulders at 1230, 1310, 1338, 1418, 1442, 1578, and
 18 1600 cm^{-1} as marked black dashed lines in Figure 4a
 19 are related to the stretching modes of the alkoxy or biphenyl
 20 group, which are presumably induced by difference in
 21 charge distribution between the saddle S_0 and planer T_1
 22 states (Figure S29, S30). The time-dependent evolution of
 23 the peak intensity at 1489 cm^{-1} is shown in Fig. 4d.
 24 Analysis of the time-dependent evolution and decay at
 25 each characteristic peak indicated the same molecular
 26 dynamics as those observed in the transient visible
 27 transmission spectroscopy (Figure S6-S9). Namely, a
 28 saddle-to-flat conformational change of the π -COT core
 29 unit in 2 ps and the relaxation to S_0 in $\tau_1 = 10$ -20, $\tau_2 = 150$
 30 ps and longer timescale. Since the 10-20 ps decay was also
 31 observed in solution phase (Figure S10), it was assigned to
 32 the relaxation dynamics of isolated molecules, which are
 33 generally located at the surface, interface or grain
 34 boundaries of the liquid crystals. In addition, the 150 ps
 35 and longer-lifetime decay modes were interpreted as the
 36 relaxation dynamics of photoexcited molecules in the LC
 37 structure. The difference in these decay modes would
 38 originate from the different local environments of excited
 39 molecules, and we assigned the long-lifetime species to the
 40 photoexcited molecule in the stacked column (see next
 41 Section).

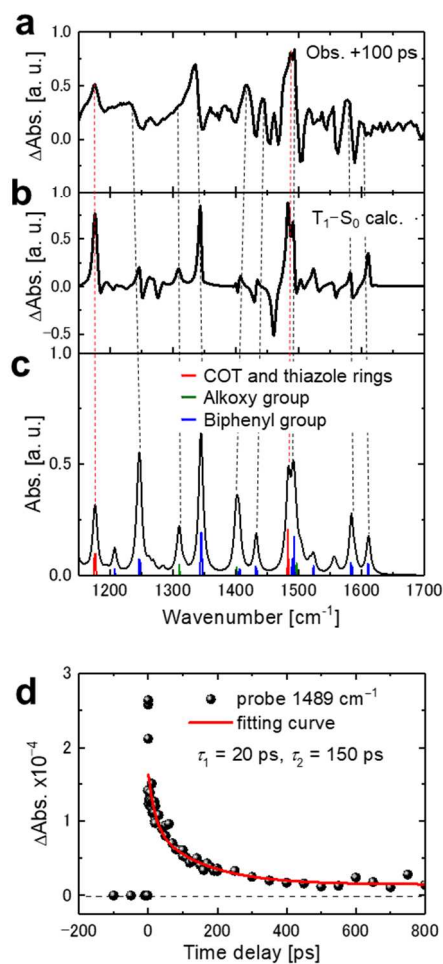


Figure 4: Ultrafast time-resolved IR spectroscopy of a π -COT-based LC thin film. **a**, **b**, Differential IR vibrational spectrum measured with a time-delay of 10 ps compared to the calculated differential vibrational spectrum (T_1 - S_0). The scaling factor of the calculated spectra is 0.97. **c**, Vibrational peak assignment of the T_1 spectrum. The peaks are classified as vibrational modes of COT and thiazole rings, alkoxy group or biphenyl group. **d**, Time evolution of the peak intensity at the representative wavenumber of 1489 cm^{-1} . The fast (20 ps) and slow (150 ps) decays are identical to the dynamics observed in isolated molecules and molecules in the LC phase.

Structural observation of the photoexcited liquid crystal.

The electron diffraction measurements were performed on a ~ 100 -nm-thick LC thin film in transmission geometry. The two-dimensional electron diffraction patterns of the LC thin film showed an ill-defined broad halo ring originating from the long alkyl chains (Figure 5a), similar to the wide XRD peak observed at diffraction angle $2\theta \approx 20^\circ$ (Figure 1b). This broad halo, which is typically observed in columnar LC materials, is composed of a number of diffraction peaks produced by the long alkyl chains and several peaks originating from the stacked π -COT core moieties. Under photoirradiation, structural deformation is induced around the photoresponsive π -COT core moieties, and then small peak modulation occurs in the diffraction pattern. By subtracting the initial diffraction

pattern from that obtained 500 ps after UV pulse irradiation, we extracted the modulated diffraction pattern induced by the UV irradiation. The resulting differential diffraction pattern was well defined with clearly observable rings (Figure 5b). Radial averages of the differential diffraction patterns at -50, 100, 300 and 500 ps after the UV pulse irradiation are presented in Figure 6a. The signal-to-noise ratio can be drastically modified by the subtraction of the diffraction pattern before the photoexcitation from that after the photoexcitation, in which negative and positive peaks are obtained. (See Figure S16 in more detail). In the differential time-resolved electron diffractometry, molecular dynamics in periodic structures can be detected sensitively rather than the dynamics of isolated molecules. Therefore, the conformational dynamics of excited molecules in the stacked column can be selectively monitored. The negative peaks (marked with blue arrows) originate from the initial structure that disappeared upon photoirradiation, while the positive peaks (marked with red arrows) indicate the formation of a new ordered structure. Since the time-evolution was relatively slow, the packing deformation should be induced by the long-lifetime species observed in the spectroscopic measurements.

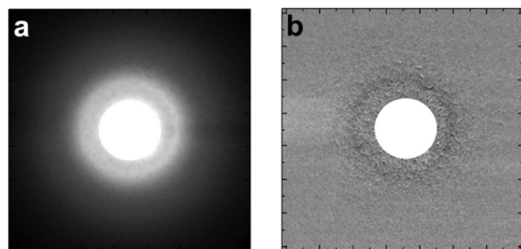


Figure 5: Electron diffraction patterns from a π -COT-based LC thin film. **a**, The electron diffraction pattern without photoexcitation. **b**, Differential diffraction pattern obtained with and without photoexcitation.

To understand the structural dynamics observed by the time-resolved electron diffraction, we performed MD simulations. To prepare suitable model for MD simulations, we considered the number of incident photons (1.2 mJ/cm²) and molecules per unit area in advance. Approximately 25% of the π -COT molecules absorb UV light and undergo the electronic transition leading to the lowest excited state. Among them, 7–8% of the photoexcited molecules (at most 2% of all the molecules of the material) remain in the excited state (Ex) even after 300–500 ps as observed in the time-resolved visible and mid-IR spectroscopies in Figures 3b and 4c, which is corresponding to the third term in the equation (1). Considering this situation, the differential electron diffraction patterns were simulated for the stacked π -COT core moieties containing small ratio of excited species (%ex), in which this percentage was set to be 20, 6.7, 4.0, and 2.9%ex (Figure S17). Here, we first considered two sets of stacked π -COT pentamers arranged with the order of saddle-saddle-flat-saddle-saddle conformers (S_0 - S_0 -Ex- S_0 - S_0) with 20%ex and all saddle conformers (S_0 - S_0 - S_0 - S_0 - S_0) with 0%ex, then these pentamers were mixed at respective ratios in the columnar stacking structure (See

details in Methods and Supplementary Section V). Shape of the simulated diffraction patterns were almost constant with 2.9, 4.0, and 6.7%ex, although the peak intensity was dependent on this percentage (Figure 6b and Figure S17). The MD simulation well reproduced most of the peaks experimentally observed in the differential electron diffractometry (Figure 6a).

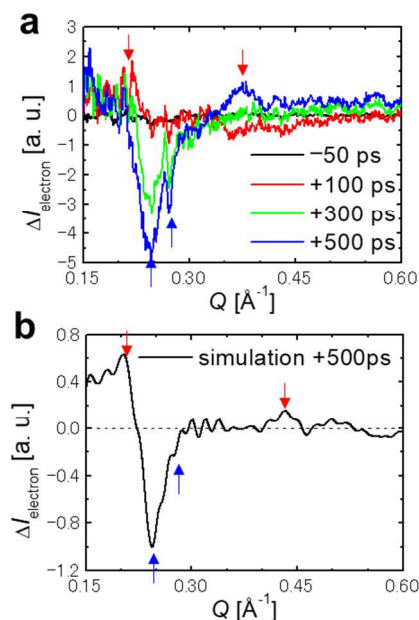


Figure 6: Ultrafast time-resolved electron diffraction of a π -COT-based LC thin film. **a**, Differential electron diffraction pattern at -50, 100, 300, and 500 ps. Red and blue arrows indicate positive and negative peaks. **b**, Simulated differential electron diffraction pattern on the basis of the MD calculation of columnar π -stacked structure containing 2.9% of excited molecules.

Combinational analysis of the time-resolved electron diffractometry and the MD simulation suggested that the conformational planarization takes place more slowly ($\tau \sim 300$ ps) for the excited molecules sandwiched by the saddle-shaped molecules (Figure 7a), and that the planarized molecule and neighboring unexcited molecules starts to rotate (from $t \sim 200$ ps with $\tau \sim 125$ ps) toward opposite direction in the stacked column due to the steric repulsion between them (Figures 7b and 8). In this columnar structure, intermolecular distance along the c -axis was determined as 4.55 Å through fitting of experimental (Figure 6a) and simulated (Figure 6b) differential diffraction patterns, then the π -stacking distance ($d_{\pi-\pi}$) between the biphenyl moieties was estimated as 3.7 Å. The dynamics of the negative peak (Figure 7a; $Q = 0.245 \text{ \AA}^{-1}$) suggested the local destruction of the π -stacked molecular ordering by the conformational planarization of excited species, starting just after the photoexcitation with the time constant of 300 ps. On the other hand, the dynamics of the broad positive peak (Figure 7b; $Q = 0.37 \text{ \AA}^{-1}$) starting to increase after 200 ps from the photoexcitation suggested the rotation of the planar excited molecule and the neighboring saddle molecules. This rotational behavior was induced by an

intermolecular steric repulsion between the rigid biphenyl moieties (Figure 8). As a result, both the conformational planarization of the π -COT molecule and the subsequent packing deformation were directly evidenced by diffractometry, strongly supporting the exhibition of the Baird aromaticity in the excited state.

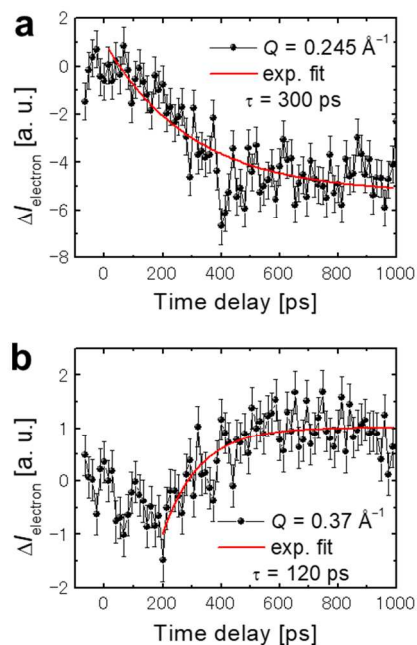


Figure 7: Time evolution of the electron diffraction peaks at the Q -values of 0.245 (a) and 0.37 \AA^{-1} (b). Here, the Q -value is defined as the reciprocal number of the lattice distance (d).

Conclusion

In conclusion, structural monitoring of fast conformational planarization of π -expanded COT molecules in the excited state has been realized in a columnar LC phase. The excited-state aromaticity exerted in the short-lived species was strongly evidenced experimentally and theoretically. The molecular motion triggered by the excited-state aromaticity produces a nanoscale torque for subsequent structural deformation in a condensed phase, which can be used as the working mechanism of photoresponsive materials.^{14,26} The insights obtained here hold out the prospect that the excited-state aromaticity will be a key concept for designing new photofunctional soft materials^{3a}.

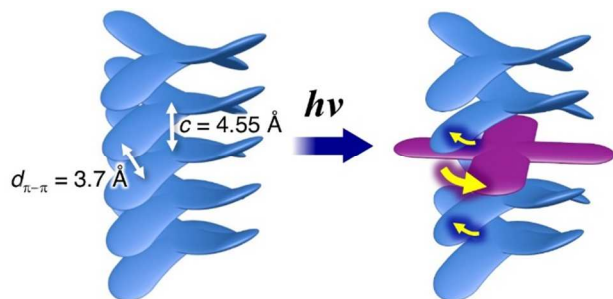


Figure 8: Structural dynamics of the photoexcited columnar LC. The dynamics of the columnar LC structure were observed using time-resolved electron diffraction. The white arrows

indicate the periodicity of the stacked molecules (4.55 \AA) as well as the π -stacking distance between the biphenyl moieties (3.7 \AA). The yellow arrows indicate the displacement of molecules.

Methods

UV-Vis transient absorption spectroscopy

We performed the conventional transient absorption spectroscopy on the π -COT molecule in LC phase. The pump pulses are modified its photon energy into 400 or 266 nm by BBO crystal(s). The probe pulse is focused into a sapphire window to generate white light (500–700 nm). The two optical pulses are focused onto the sample, and the transmitted white probe light is dispersed by the spectrometer and detected with the Si photodiode. The incident fluence of the pump light was 1 mJ/cm^2 . The sample was spread on bulk CaF_2 substrate, melt at 100 $^\circ\text{C}$ on a hotplate, and cooled gradually to room temperature.

Time-resolved mid-IR vibrational spectroscopy

UV (266 nm) pump and mid-IR (1050–1700 cm^{-1}) probe time-resolved spectroscopy were performed in the transmission mode on π -COT molecule in solution (1 mM in CH_2Cl_2 solvent) and in LC phase coated on CaF_2 substrate. The experimental details of this optical pump-probe setup are presented elsewhere²⁵. The incident angle of the pump and probe light was set nearly parallel to the surface normal of the sample. The pulse durations of the UV and mid-IR pulses were 100 fs and <1 ps, respectively. The repetition rate and the incident fluence of the UV pump pulse were 500 Hz and 1 mJ/cm^2 , respectively.

Time-resolved electron diffraction

The experimental setup of the compact DC-accelerated electron diffraction is provided elsewhere²⁷. UV (266 nm) pump was focused to a 210- μm spot size on the \sim 100 nm thick film of π -COT molecule. The incident laser fluence was 1.2 mJ/cm^2 . From the transmission and reflectivity of the sample measured to be 40% and 30% respectively, absorption fluence was determined to be 0.36 mJ/cm^2 . The acceleration voltage of the probe electron pulses was 75 keV under a DC electric field. Photoinduced structural changes inside the material were investigated with electron pulses containing 2×10^4 electrons (3 fC) confined to a 100- μm -diameter spot incident on the sample. The UV optical pulse to generate electrons was stretched to be >500 fs by a 25-mm-thick fused silica plate on purpose. The pulse duration of the electron beam was \sim 1 ps. Diffracted and directly transmitted electrons were focused with a magnetic lens onto a 1:2 fiber-coupled charge-coupled device camera coated with a P43 ($\text{Gd}_2\text{O}_2\text{S}:\text{Tb}$) phosphor scintillator. To acquire one electron diffraction image, 1×10^4 shots of electron pulses were collected at repetition rates of 500 Hz. The sample solution in chloroform (10 mg/ml) was spin-coated on SiN thin (30 nm) membrane. The thin sample film was melt on a hotplate, and cooled gradually to room temperature.

Synthesis

The π -COT-based LC compound was synthesized by the Suzuki-Miyaura cross coupling reaction of cyclic 2-(4-chlorophenyl)thiazole tetramer and the 3,4,5-tridodecyloxyphenyl boronic acid using Pd₂(dba)₃·CHCl₃ and the Buckwald phosphine ligand of XPhos²⁸. Purification was performed by repeated silica gel column chromatography and high performance liquid chromatography (HPLC). The isolated yield was 78% (see the Supplementary Section I).

Density functional theory (DFT) calculations

The energy profile of the π -COT core unit was calculated at B3LYP/6-31+G* level using Gaussian09²⁹, in which the structural restraint was set by the modredundant keyword with the structural symmetry of C₂. In addition to the DFT calculations, the full structural optimizations in S₀, S₁, T₁ and T₂ of a π -COT were performed in CASSCF(8, 8)/6-31G* level using Gaussian09. The NICS ((U)B3LYP/6-311+G*) and HOMA values were calculated using the DFT or CASSCF optimized structures. The ACID plots are based on structures and wavefunctions optimized at the UB3LYP/6-31+G* level of density functional theory. The ACID scalar fields were calculated using our program at an isosurface value of 0.03.^{20,30}

Molecular dynamics (MD) simulation

We performed the MD simulations of stacked models of the π -COT core unit (Supplementary Section VI) to investigate structural changes due to excitation in a condensed phase. We first prepared two model structures, *i.e.* (A) all saddle-shaped conformers (5 molecules), that consist of a S₀-S₀-S₀-S₀-S₀ pentamer, and (B) a mixture of saddle-shaped (S₀) and flat (T₁ as Ex) conformers (35 molecules). In the model (B), the flat conformers were placed every 5 molecules, meaning that seven sets of the S₀-S₀-Ex-S₀-S₀ pentamer were periodically aligned. After the MD calculations, a set of the S₀-S₀-Ex-S₀-S₀ pentamer at the center of the super cell was selected and mixed with the S₀-S₀-S₀-S₀-S₀ pentamer for the simulated diffraction analysis in Figure 4d and Figures S17-18. In the MD calculations, the temperature of the system was gradually increased from 0 K to 300 K for 20 ps, and then the additional equilibration was subsequently performed for 1 ns with the NVT ensemble (T = 300 K and V = 19.0×19.0×31.1 Å³ for (A) and 21.5×21.5×186.7 Å³ for (B), respectively) under the three-dimensional periodic boundary condition. Finally, the production runs were performed for 1 ns with the NVT ensemble. During the MD simulations, several types of restraints were imposed to keep the stacked structures (see Supporting information VI for details). Throughout this study, all the MD calculations were performed by the Amber 14 program suite,³¹ where the AMBER force field of the S₀ and T₁ states for the π -COT core unit were generated by the Antechamber tool from the Gaussian outputs at B3LYP/6-31G*.

ASSOCIATED CONTENT

Supporting information is available free of charge on the ACS Publishing website at DOI:
Synthesis of π -COT: Fig. S1, S2

Static characterization: Fig. S3, S4, Table S1
Optical measurements: Fig. S5-S9
Mid-IR vibrational spectroscopy: Fig. S10-S15, Table S2, S3
Time-resolved electron diffraction: Fig. S16-S18, Table S4-S7
Calculations: Fig. S19-S34, Table S8-S25

AUTHOR INFORMATION

Corresponding Authors

hadamasaki@okayama-u.ac.jp, s_saito@kuchem.kyoto-u.ac.jp,
shigeta@ccs.tsukuba.ac.jp, konda@chem.kyushu-univ.jp

Funding Sources

Japan Science Technology Agency (JST), PRESTO, Grant numbers: JPMJPR13KD, JPMJPR12K5, JPMJPR16P6.
JSPS KAKENHI, Grant Numbers: JP15H02103, JP17K17893, JP15H05482, JP17H05258, JP26107004, JP17H06375

ACKNOWLEDGMENT

We thank Prof. Takashi Kato at the University of Tokyo, Prof. Yoshiaki Uchida at Osaka University, Prof. Shin-ya Koshihara at Tokyo Institute of Technology for valuable discussions, Dr. Sercan Keskin at the University of Hamburg for the measurement of static electron diffraction, and Dr. Yumi Nakaike for the measurement of DSC.

REFERENCES

- Baird, N. C. *J. Am. Chem. Soc.* **1972**, *94*, 4941-4948.
- Hückel, E. *Z. Physik* **1931**, *70*, 204-286.
- (a) Ottosson, H. *Nat. Chem.* **2012**, *4*, 969-971. (b) Rosenberg, M.; Dahlstrand, C.; Kilså, K.; Ottosson, H. *Chem. Rev.* **2014**, *114*, 5379-5425. (c) Gogonea, V.; Schleyer, P. V. R.; Schreiner, P. R. *Angew. Chem. Int. Ed.* **1998**, *37*, 1945-1948.
- (a) Heilbronner, E. *Tetrahedron Lett.* **1964**, *5*, 1923-1928. (b) Mauksch, M.; Gogonea, V.; Jiao, H.; von Ragué Schleyer, P. *Angew. Chem. Int. Ed.* **1998**, *37*, 2395-2397. (c) Ajami, D.; Oeckler, O.; Simon, A.; Herges, R. *Nature* **2003**, *426*, 819-821. (d) Herges, R. *Chem. Rev.* **2006**, *106*, 4820-4842. (e) Tanaka, Y.; Saito, S.; Mori, S.; Aratani, N.; Shinokubo, H.; Shibata, N.; Higuchi, Y.; Yoon, Z. S.; Kim, K. S.; Noh, S. B.; Park, J. K.; Kim, D.; Osuka, A. *Angew. Chem. Int. Ed.* **2008**, *47*, 681-684. (f) Yoon, Z. S.; Osuka, A.; Kim, D. *Nat. Chem.* **2009**, *1*, 113-122. (g) Saito, S.; Osuka, A. *Angew. Chem. Int. Ed.* **2011**, *50*, 4342-4373. (h) Stepień, M.; Sprutta, N.; Latos-Grażyński, L. *Angew. Chem. Int. Ed.* **2011**, *50*, 4288-4340.
- (a) Corminboeuf, C.; Schleyer, P. V. R.; Warner, P. *Org. Lett.* **2007**, *9*, 3263-3266. (b) Bean, D. E.; Fowler, P. W. *Org. Lett.* **2008**, *10*, 5573-5576. (c) Nozawa, R.; Tanaka, H.; Cha, W.-Y.; Hong, Y.; Hisaki, I.; Shimizu, S.; Shin, J.-Y.; Kowalczyk, T.; Irlle, S.; Kim, D.; Shinokubo, H. *Nat. Commun.* **2016**, *7*, 12094.
- (a) Wan, P.; Krogh, E. *J. Chem. Soc. Chem. Commun.* **1985**, 1207-1208. (b) Shukla, D.; Wan, P. *J. Am. Chem. Soc.* **1993**, *115*, 2990-2991. (c) Möllerstedt, H.; Piqueras, M. C.; Crespo, R.; Ottosson, H. *J. Am. Chem. Soc.* **2004**, *126*, 13938-13939. (d) Wörner, H. J.; Merkt, F. *Angew. Chem. Int. Ed.* **2006**, *45*, 293-296.
- (a) Sung, Y. M.; Yoon, M.-C.; Lim, J. M.; Rath, H.; Naoda, K.; Osuka, A.; Kim, D. *Nat. Chem.* **2015**, *7*, 418-422. (b) Ottosson, H. *Nat. Chem.* **2015**, *7*, 373-375. (c) Sung, Y. M.; Oh, J.; Kim, W.; Mori, H.; Osuka, A.; Kim, D.; *J. Am. Chem. Soc.*, **2015**, *137*, 11856-11859. (d) Oh, J.; Sung, Y. M.; Kim, W.; Mori, S.; Osuka, A.; Kim, D. *Angew. Chem. Int. Ed.* **2016**, *55*, 6487-6491. (e) Sung, Y. M.; Oh, J.; Naoda, K.; Lee, T.; Kim, W.; Lim, M.; Osuka, A.; Kim, D. *Angew. Chem. Int. Ed.* **2016**, *55*, 11930-11934. (f) Hong, Y.; Oh, J.; Sung, Y. M.; Tanaka, Y.; Osuka, A.; Kim, D. *Angew. Chem. Int. Ed.* **2017**, *56*, 2932-2936.
- Ueda, M.; Jorner, K.; Sung, Y. M.; Mori, T.; Xiao, Q.; Kim, D.; Ottosson, H.; Aida, T.; Itoh, Y. *Nat. Commun.* **2017**, *8*, 346.

9. (a) Beaud, P.; Caviezel, A.; Mariager, S. O.; Rettig, L.; Ingold, G.; Dornes, C.; Huang, S.-W.; Johnson, J. A.; Radovic, M.; Huber, T.; Kubacka, T.; Ferrer, A.; Lemke, H. T.; Chollet, M.; Zhu, D.; Glownia, J. M.; Sikorski, M.; Robert, A.; Wadati, H.; Nakamura, M.; Kawasaki, M.; Tokura, Y.; Johnson S. L.; Staub, U. *Nat. Mater.* **2014**, *13*, 923–927. (b) Minitti, M. P.; Budariz, J. M.; Kirrander, A.; Robinson, J. S.; Ratner, D.; Lane, T. J.; Zhu, D.; Glownia, J. M.; Kozina, M.; Lemke, H. T.; Sikorski, M.; Feng, Y.; Nelson, S.; Saita, K.; Stankus, B.; Northey, T.; Hastings, J. B.; Weber, P. M. *Phys Rev. Lett.* **2015**, *114*, 255501. (c) Kim, K. H.; Kim, J. G.; Nozawa, S.; Sato, T.; Oang, K. Y.; Kim, T. W.; Ki, H.; Jo, J.; Park, S.; Song, C.; Sato, T.; Ogawa, K.; Togashi, T.; Tono, K.; Yabashi, M.; Ishikawa, T.; Kim, J.; Ryoo, R.; Kim, J.; Ihee, H.; Adachi, S. *Nature* **2015**, *518*, 385–389. (d) Ishikawa, T.; Aoyagi, H.; Asaka, T.; Asano, Y.; Azumi, N.; Bizen, T.; Ego, H.; Fukami, K.; Fukui, T.; Furukawa, Y.; Goto, S.; Hanaki, H.; Hara, T.; Hasegawa, T.; Hatsui, T.; Higashiya, A.; Hirono, T.; Hosoda, N.; Ishii, M.; Inagaki, T.; Inubushi, Y.; Itoga, T.; Joti, Y.; Kago, M.; Kameshima, T.; Kimura, H.; Kirihara, Y.; Kiyomichi, A.; Kobayashi, T.; Kondo, C.; Kudo, T.; Maesaka, H.; Maréchal, X. M.; Masuda, T.; Matsubara, S.; Matsumoto, T.; Matsushita, T.; Matsui, S.; Nagasono, M.; Nariyama, N.; Ohashi, H.; Ohata, T.; Ohshima, T.; Ono, S.; Otake, Y.; Saji, C.; Sakurai, T.; Sato, T.; Sawada, K.; Seike, T.; Shirasawa, K.; Sugimoto, T.; Suzuki, S.; Takahashi, S.; Takebe, H.; Takeshita, K.; Tamasaku, K.; Tanaka, H.; Tanaka, R.; Tanaka, T.; Togashi, T.; Togawa, K.; Tokuhisa, A.; Tomizawa, H.; Tono, K.; Wu, S.; Yabashi, M.; Yamaga, M.; Yamashita, A.; Yanagida, K.; Zhang, C.; Shintake, T.; Kitamura H.; Kumagai, N. *Nat. Photon.* **2012**, *6*, 540–544.
10. (a) Morrison, V. R.; Chatelain, R. P.; Tiwari, K. L.; Hendaoui, A.; Bruhács, A.; Chaker, M.; Siwick, B. J. *Science* **2014**, *346*, 445–448. (b) Gao, M.; Lu, C.; Jean-Ruel, H.; Liu, L. C.; Marx, A.; Onda, K.; Koshihara, S.; Nakano, Y.; Shao, X.; Hiramatsu, T.; Saito, G.; Yamochi, H.; Cooney, R. R.; Moriena, G.; Sciaini, G.; Miller, R. J. D. *Nature* **2013**, *496*, 343–346. (c) Ishikawa, T.; Hayes, S. A.; Keskin, S.; Corthey, G.; Hada, M.; Pichugin, K.; Marx, A.; Hirscht, J.; Shionuma, K.; Onda, K.; Okimoto, Y.; Koshihara, S.; Yamamoto, T.; Cui, H.; Nomura, M.; Oshima, Y.; Abdel-Jawad, M.; Kato, R.; Miller, R. J. D. *Science* **2015**, *350*, 1501–1505. (d) Zewail, A. H. *Science* **2010**, *328*, 187–193. (e) Miller, R. J. D. *Science* **2014**, *343*, 1108–1116.
11. (a) Andrew, T. L.; Swager, T. M. *Macromol.* **2008**, *41*, 8306–8308. (b) Schols, S.; Kadashchuk, A.; Heremans, P.; Helfer, A.; Scherf, U. *ChemPhysChem* **2009**, *10*, 1071–1076.
12. (a) Zheng, Q.; Jockusch, S.; Rodríguez-Calero, G. G.; Zhou, Z.; Zhao, H.; Altman, R. B.; Abruña, H. D.; Blanchard, S. C. *Photochem. Photobiol. Sci.* **2016**, *15*, 196. (b) Dave, R.; Terry, D. S.; Munro, J. B.; Blanchard, S. C. *Biophys. J.* **2009**, *96*, 2371–2381.
13. Kotani, R.; Sotome, H.; Okajima, H.; Yokoyama, S.; Nakaike, Y.; Kashiwagi, A.; Mori, C.; Nakada, Y.; Yamaguchi, S.; Osuka, A.; Sakamoto, A.; Miyasaka, H.; Saito, S. *J. Mater. Chem. C* **2017**, *5*, 5248–5256.
14. Saito, S.; Nobusue, S.; Tsuzaka, E.; Yuan, C.; Mori, C.; Hara, M.; Seki, T.; Camacho, C.; Irle, S.; Yamaguchi, S. *Nat. Commun.* **2016**, *7*, 12094.
15. Goodby, J. W.; Collings, P. J.; Kato, T.; Tschierske, C.; Gleeson, H. F.; Raynes, P.; Eds., *Handbook of Liquid Crystals* (Wiley-VCH, Weinheim, Germany, 2014).
16. Mouri, K.; Saito, S.; Yamaguchi, S. *Angew. Chem. Int. Ed.* **2012**, *51*, 5971–5975.
17. Karadakov, P. B. *J. Phys. Chem. A* **2008**, *112*, 12707–12713.
18. Garavelli, M.; Bernardi, F.; Cembran, A.; Castaño, O.; Frutos L.M.; Merchán M.; Olivucci, M. *J. Am. Chem. Soc.* **2002**, *124*, 13770–13789.
19. (a) Forward, P. J.; Gorman, A. A.; Hamblett, I. *J. Chem. Soc., Chem. Commun.* **1993**, 250–251. (b) Das, T. N.; Priyadarsini, K. I. *J. Chem. Soc. Faraday Trans.* **1994**, *90*, 963–968. (c) Frutos, L.-M.; Castaño, O.; Andrés, J. L.; Merchán, M.; Acuña, A. U. *J. Chem. Phys.* **2004**, *120*, 1208–1216.
20. Geuenich, D.; Hess, K.; Köhler, F.; Herges, R. *Chem. Rev.* **2005**, *105*, 3758–3772.
21. (a) Chen, Z.; Wannere, C. S.; Corminboeuf, C.; Puchta, R.; Schleyer, P. v. R. *Chem. Rev.* **2005**, *105*, 3842–3888. (b) Schleyer, P. v. R.; Manoharan, M.; Wang, Z.-X.; Kiran, B.; Jiao, H.; Puchta, R.; Hommes, N. J. R. v. E. *Org. Lett.* **2001**, *3*, 2465–2468. (c) Cernusak, I.; Fowler, P. W.; Steiner, E. *Mol. Phys.* **2000**, *98*, 945–953. (d) F.-B.-S. Hossein, Wannere, C. S.; Corminboeuf, C.; Puchta, R.; Schleyer, P. v. R. *Org. Lett.* **2006**, *8*, 863–866.
22. Krygowski, T. M.; Cyrński, M. K. *Chem. Rev.* **2001**, *101*, 1385–1419.
23. Ayub, R.; Bakouri, O. E.; Jorner, K.; Solà, M.; Ottosson, H. *J. Org. Chem.* **2017**, *82*, 6327–6340.
24. Paik, D. H.; Yang, D.-S.; Lee I-R.; Zewail A. H. *Angew. Chem. Int. Ed.* **2004**, *43*, 2830–2834.
25. (a) Mukuta, T.; Fukazawa, N.; Murata, K.; Inagaki, A.; Akita, M.; Tanaka, S.; Koshihara, S.; Onda, K. *Inorg. Chem.* **2014**, *53*, 2481–2490. (b) Tanaka, S.; Takahashi, K.; Hirahara, M.; Yagi, M.; Onda, K. *J. Photochem. Photobiol. A* **2015**, *313*, 87–98. (c) Mukuta, T.; Tanaka, S.; Inagaki, A.; Koshihara, S.; Onda, K. *ChemistrySelect* **2016**, *1*, 2802–2807.
26. (a) Ikeda, T.; Mamiya, J.; Yu, Y. *Angew. Chem. Int. Ed.* **2007**, *46*, 506–528. (b) White, T. J.; Broer, D. J. *Nat. Mater.* **2015**, *14*, 1087–1098.
27. Hada, M.; Zhang, D.; Pichugin, K.; Hirscht, J.; Kochman, M. A.; Hayes, S. A.; Manz, S.; Gengler, R. Y. N.; Wann, D. A.; Seki, T.; Moriena, G.; Morrison, C. A.; Matsuo, J.; Sciaini, G.; Miller, R. J. D. *Nat. Commun.* **2014**, *5*, 3863.
28. Martin, R.; Buchwald, S. L. *Acc. Chem. Res.* **2008**, *41*, 1461–1473.
29. Frisch, M. J.; Trucks, G. W.; Schlegel, H. B.; Scuseria, G. E.; Robb, M. A.; Cheeseman, J. R.; Scalmani, G.; Barone, V.; Petersson, G. A.; Nakatsuji, H.; Li, X.; Caricato, M.; Marenich, A.; Bloino, J.; Janesko, B. G.; Gomperts, R.; Mennucci, B.; Hratchian, H. P.; Ortiz, J. V.; Izmaylov, A. F.; Sonnenberg, J. L.; Williams-Young, D.; Ding, F.; Lipparini, F.; Egidi, F.; Goings, J.; Peng, B.; Petrone, A.; Henderson, T.; Ranasinghe, D.; Zakrzewski, V. G.; Gao, J.; Rega, N.; Zheng, G.; Liang, W.; Hada, M.; Ehara, M.; Toyota, K.; Fukuda, R.; Hasegawa, J.; Ishida, M.; Nakajima, T.; Honda, Y.; Kitao, O.; Nakai, H.; Vreven, T.; Throssell, K.; Montgomery, Jr. J. A.; Peralta, J. E.; Ogliaro, F.; Bearpark, M.; Heyd, J. J.; Brothers, E.; Kudin, K. N.; Staroverov, V. N.; Keith, T.; Kobayashi, R.; Normand, J.; Raghavachari, K.; Rendell, A.; Burant, J. C.; Iyengar, S. S.; Tomasi, J.; Cossi, M.; Millam, J. M.; Klene, M.; Adamo, C.; Cammi, R.; Ochterski, J. W.; Martin, R. L.; Morokuma, K.; Farkas, O.; Foresman, J. B.; Fox, D. J. *Gaussian 09, Revision D.01 and E.01*, Gaussian, Inc., Wallingford CT, 2013.
30. Herges, R.; Geuenich, D. *Phys. Chem. A* **2001**, *105*, 3214–3220.
31. Case, D.A.; Cerutti, D.S.; Cheatham, III, T.E.; Darden, T.A.; Duke, R.E.; Giese, T.J.; Gohlke, H.; Goetz, A.W.; Greene, D.; Homeyer, N.; Izadi, S.; Kovalenko, A.; Lee, T.S.; LeGrand, S.; Li, P.; Lin, C.; Liu, J.; Luchko, T.; Luo, R.; Mermelstein, D.; Merz, K.M.; Monard, G.; Nguyen, H.; Omelyan, L.; Onufriev, A.; Pan, F.; Qi, R.; Roe, D. R.; Roitberg, A.; Sagui, C.; Simmerling, C. L.; Botello-Smith, W. M.; Swails, J.; Walker, R. C.; Wang, J.; Wolf, R. M.; Wu, X.; Xiao, L.; York D. M.; Kollman, P.A. *AMBER14*, University of California, San Francisco, 2014.